Morphometric Analysis of Lipoprotein-like Particle Accumulation in Aging Human Macular Bruch's Membrane

Jiahn-Dar Huang,[1] *Christine A. Curcio,*[2] *and Mark Johnson*[1]

Purpose. To determine the size and regional distribution of lipoprotein-like particles (LLPs) that accumulate with age in Bruch's membrane (BrM).

Methods. The quick-freeze/deep-etch method was used to prepare specimens of human BrM (age range, 27–78) for electron microscopic examination. Stereologic methods were used to analyze the resultant micrographs and determine the age-related changes of the LLP volume fraction and diameter distribution in various locations in BrM.

Results. The volume fraction occupied by LLPs was found to increase monotonically with age in both the inner collagenous layer (ICL) and elastic layer (EL), but not in the outer collagenous layer (OCL). The mass of total LLP-associated lipids in BrM also increased with age. There was no significant increase in LLP size with age, but there was a modest increase in size with increased volume fraction of LLPs in BrM.

Conclusions. The pattern of accumulation of particles was consistent with a retinal pigment epithelium (RPE) source for the LLPs, which explains why once the EL and ICL were filled with particles, LLPs continued to accumulate near the RPE, but no further accumulation was found in the OCL. The quantity of LLP-associated lipids found in BrM accounts for a large portion of the accumulated lipids measured in this tissue. (*Invest Ophthalmol Vis Sci.* 2008;49:2721–2727) DOI:10.1167/iovs.07-1196

Bruch's membrane (BrM) is a thin layer of connective tissue located between the retinal pigment epithelium (RPE) and choroid. This tissue collects abundant quantities of lipid-rich deposits with advancing age.[1–5] Higher quantities of lipid deposits are found in the macular region,[2,3,6] and these deposits are postulated to compromise the metabolic transport through this region, which is important for the health of RPE and photoreceptor cells.[4,7–12]

From the [1]Department of Biomedical Engineering, Northwestern University, Evanston, Illinois; and the [2]Department of Ophthalmology, University of Alabama School of Medicine, Birmingham, Alabama.

Presented at the annual meetings of the Association for Research in Vision and Ophthalmology, Fort Lauderdale, Florida, May 2006 and 2007.

Supported by National Eye Institute Grants EY014662 and EY06109, the American Health Assistance Foundation, the International Retina Research Foundation, and Research to Prevent Blindness, Inc. (to the Department of Ophthalmology at The University of Alabama School of Medicine, Birmingham, AL).

Submitted for publication September 13, 2007; revised February 6, 2008; accepted April 11, 2008.

Disclosure: **J.-D. Huang**, None; **C.A. Curcio**, None; **M. Johnson**, None

The publication costs of this article were defrayed in part by page charge payment. This article must therefore be marked "*advertisement*" in accordance with 18 U.S.C. §1734 solely to indicate this fact.

Corresponding author: Mark Johnson, Department of Biomedical Engineering, Northwestern University, 2145 Sheridan Road, Evanston, IL 60208-3107; m-johnson2@northwestern.edu.

In our previous studies, we used the quick-freeze/deep-etch (QFDE) technique, a method that preserves the ultrastructure of BrM to characterize the age-related changes in the tissue.[4–6] We found that two major types of deposits, lipoprotein-like particles (LLPs) and small granules (SGs), accumulate with age in BrM.[5] LLPs were of particular interest because they are a lipid-rich material.[5,13]

Our previous work[4–5] suggested that the age-related accumulation of LLPs in BrM first fills the interfibrillar spacing of the elastic layer (EL) and then progressively fills the inner collagenous layer (ICL), ultimately leading to the formation of a "lipid wall" between the ICL and the basal lamina of the RPE (BL-RPE). Although LLPs were found in the outer collagenous layer (OCL) in younger eyes, no further age-related accumulation was seen in this region. These observations suggested that the source of the LLPs was in the RPE.

The goal in the present study was to examine this result quantitatively. We used stereologic methods to determine the volume fraction of LLPs seen in the images of the ICL, EL, and OCL prepared by QFDE. As our previous studies indicated that the LLP sizes were not uniform and that the LLPs were capable of fusing to form larger particles,[5] we also determined the particle diameter distribution in each of the three central layers of BrM. These studies allowed us to demonstrate the age-related variations of the LLPs in human macular BrM.

Materials and Methods

Human Eye Tissue

Human eye tissues used in this study were obtained from the Alabama Eye Bank and preserved within 4 hours after death. Eyes containing drusen larger than 63 μm or any other grossly visible chorioretinal disease of significance were excluded. In addition, we excluded eyes from donors with diabetes or receiving artificial respiration longer than 5 days. Twelve normal eyes, aged from 27 to 78 years, with 2 eyes from each decade of human life, as previously described,[5] were analyzed (Table 1).

Tissue Processing

After the removal of the anterior segment of each eye, the posterior segment was preserved by immersion in 0.1 M phosphate-buffered solution, with 2.5% glutaraldehyde and 1% paraformaldehyde, for at least 24 hours. The macular region (an 8 × 8-mm area) of each eye was sampled in the present study. We dissected the macular region, including the retina, RPE, BrM, choroid, and sclera into sixteen 2 × 2-mm square blocks for QFDE and thin-section processing.

For tissue blocks processed by QFDE (6–12 blocks per eye), the retina was carefully removed from the tissue by using fine forceps. The remaining RPE–BrM–choroid–sclera complex was flash frozen in liquid nitrogen (−196°C; model EM MM80E Leica Microsystems Inc., Bannockburn, IL). The frozen tissue was then transferred, with the RPE side facing up, into a freeze-fracture/deep-etch device (model CFE-60; Cressington Scientific Instruments Ltd., Watford, UK), held at a vacuum level of 10^{-7} mbar. The tissue block was

TABLE 1. Sample Eyes

Donor Age	Sex	Ethnicity
27	F	AA
29	M	C
34	F	C
35	F	C
45	M	C
50	M	C
53	M	C
58	F	C
63	M	C
64	M	AA
77	F	C
78	M	C

F, female; M, male; C, Caucasian; AA, African American.

fractured at low oblique angles with a cold razor blade and then etched at −95°C for 25 minutes to reveal BrM. Rotary shadowing with a platinum–carbon mixture at 20° to the tissue surface and backed by carbon from above was used to make a replica of exposed BrM ultrastructure. The replica, along with the tissue, was immersed in the digestion solution (water/bleach = 1:1) for at least 2 hours, to remove the biological tissue. The remaining replica pieces were picked up by copper hexagonal grids, washed in water, air dried, and examined (model 100 CX; JEOL USA, Peabody, MA) using a transmission electron microscope. Stereo micrograph pairs (±6°) of a ×8000 original magnification of the QFDE replica were scanned (Duoscan T2500; Agfa, Orangeburg, NY) in TIFF mode. To improve image contrast, we used image-management software (Photoshop CS; Adobe Systems Inc., San Jose, CA) to equalize the digitized images.

Thin-sectioning transmission electron microscopy (TEM) preparation was also used for one or two tissue blocks of each eye. In this preparation, the fixed tissue blocks were postfixed either in 1% osmium and 0.125% potassium ferricyanide or by osmium-tannic acid-paraphenylenediamine (OTAP).[14] One-micrometer-thick sections of the tissue were stained with 1% toluidine-blue-O in 2% sodium borohydrate. We then examined the thin sections by TEM (1200 EXII; JEOL USA, or a model 7000; Hitachi High Technology America, Pleasanton, CA). Representative negatives of BrM cross sections (EM film 4489; Eastman-Kodak, Rochester, NY) were scanned (PowerLook 1100 scanner and Magiscan 4.5; Umax Technology, Dallas TX).

Image Processing and Stereologic Analysis

Since very few LLPs were observed in the BL-RPE and the basal lamina of the choriocapillaris (BL-CC),[5] only images from the ICL, EL, and OCL were selected for LLP quantification. The layers of BrM revealed by QFDE were not always continuous,[5] and thus, morphometric analysis of each of the three layers (ICL, EL, and OCL) was not always possible for each tissue block. For each layer of each eye, at least three QFDE images were used to evaluate the LLP volume fraction seen in that layer. The OCL images of the 50-year-old eye were not available, due to technical difficulties. Images of the lipid wall in some eyes (63, 77, and 78 years) were not included in these evaluations, as the depth of field necessary for the stereology could not be determined from the densely packed images.

The depth of field of QFDE images was greater than the characteristic size of the objects being measured in the images. As such, since the images are two-dimensional projections of a three-dimensional set of objects, stereologic correction was necessary to determine the volume fraction of LLPs in an image. Overby and Johnson[15] developed methods for determining the volume fraction of a set of three-dimensional objects (ϕ) from the volume fraction measured on two-dimensional projections of these objects (ϕ'). We used their methodology, but considered only the volume fraction of the LLPs in the images of BrM.

To determine the ϕ of the LLPs in a region, we required measurements of the fraction of the image covered by LLPs (ϕ'), including those complexes composed of LLPs and SGs, as described in the previous study,[5] the total perimeter of these particles per unit image area (α'), and the depth of field of the image (D_f). To evaluate ϕ' and α' for a particular image, we visually identified the LLPs and then traced them with a mouse. An example is shown in Figure 1. ImageJ (available by ftp at zippy.nimh.nih.gov/ or at http://rsb.info.nih.gov/nih-image; developed by Wayne Rasband, National Institutes of Health, Bethesda, MD) was then used to determine the area and perimeter of each LLP. For each micrograph, the area and perimeter of all LLPs in that micrograph were summed and then divided by the total image area, to obtain the values of ϕ' and α' of the image. The values of ϕ' and α' of each layer of each eye were determined by the weighted average of ϕ' and α' values of each image, with the image area as the weighted factor.

The detailed method to measure D_f of a QFDE image is described in Overby et al.[16] In the present study, for each EM image evaluated for ϕ' and α', three 500 × 500-nm regions were randomly selected in the image. Stereo images (±6°) of the region were overlapped (Photoshop CS; Adobe Systems). Two relatively nearby features on a micrograph were identified (within 100 nm of one another) and the distance between these two features was measured on both stereo images by using ImageJ. The difference between these two lengths (Δl) could then be related to the vertical distance between these two structures, by using the relationship $\Delta y = \Delta l/2 \sin\theta$ ($\theta = 6°$). Three such measurements were made on each of the three regions of each micrograph. The D_f of each layer of each eye was then determined as the highest value of Δy obtained in all 27 measurements in the three images of each layer.

The following equations[15] were used to relate the measured parameters to the volume fraction of the LLPs in each layer of each eye:

$$\phi' = 1 - (1 - \phi)\exp\left(\frac{-\alpha D_f}{4(1-\phi)}\right) \quad (1)$$

$$\alpha' = \frac{\alpha\pi}{4}\exp\left(\frac{-\alpha D_f}{4(1-\phi)}\right)\left(1 + \frac{2\alpha D_f}{3\pi\phi} + \frac{\alpha D_f}{4(1-\phi)}\right) \quad (2)$$

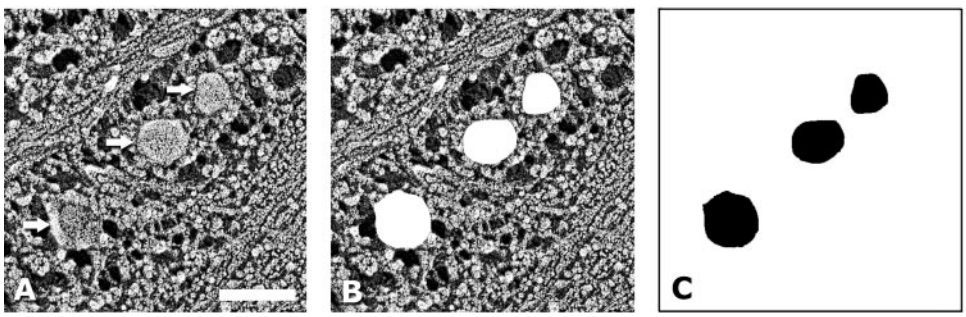

FIGURE 1. The LLPs seen in QFDE images of the EL of a 34-year-old eye. (**A**) The LLPs (*arrows*) had grayscale values similar to those of other ultrastructural features. (**B**) Particle content was cleared to make the LLPs stand out. (**C**) After inverting and thresholding the image, only the LLPs remained. Scale bar, 100 nm.

The form of equations 1 and 2 are appropriate for spherically shaped particles,[15] a reasonable approximation for LLPs. Once the values of ϕ', α', and D_f were determined, only two unknowns, ϕ and α, remained. The two unknown values were then calculated by solving equation 1 and 2 (MatLab; MathWorks, Natick, MA).

Determination of LLP Diameter and Size Distribution

Individual, nonoverlapped particles seen in the images were considered for the evaluation of the LLP diameters. This criterion excluded less than 1% of all the particles shown in the images.

The projected area of a particle (a) was measured with ImageJ. Because most of LLPs seen in BrM prepared by QFDE were not sectioned by fracturing (as determined from the particle diameter distributions such as that seen in Figure 6), stereologic correction was not used for the measured particle areas. The particle diameter D was determined from the relation: $a = \pi D^2/4$, as LLPs were considered as spheroids in the present study. The average value of D for LLPs was determined in each of the three layers (ICL, EL, and OCL) of each eye.

To determine the distribution of particle sizes, we divided the LLPs in a layer of a particular eye into groups, each of which contained particles of similar diameter in 10-nm intervals from 0 to 300 nm. To generate the diameter distribution, we divided the number of particles in each interval by the total number of LLPs in that layer of that eye. For each layer, the age-related changes in LLP diameter distribution were presented as data from three age ranges: 20 to 40, 40 to 60, and 60 to 80 years. The histogram of each age group was obtained from the average of the four eyes in that group, except the OCL of 40 to 60 years, which contained only three sample eyes.

Estimate of the Total Quantity of LLP-Associated Lipids in BrM

Holz et al.[2] reported values for the total lipid content of macular BrM and choroid. We used the morphometrically determined values of LLP size and volume in each layer to estimate the total quantity (Q) of LLP-associated lipid in BrM, for comparison to their measurements.

The total quantity of lipid the in LLPs found in BrM was estimated as

$$Q = \sum_i \phi_i \times l_i \times A \times \sigma \times 0.85 \qquad (3)$$

where i represents the individual layers of BrM (ICL, EL, and OCL), ϕ_i is the volume fraction of lipid in the ith layer, l_i is the thickness of the ith layer, A is the tissue area, and σ is the density of the LLP particles. We assumed that the density of the LLPs and the lipid-protein ratio of each LLP were similar to the average of LDL and VLDL.[17–20] Therefore, σ was set a 1 g/mL, and the constant 0.85 was used as an estimate of the lipid fraction of an LLP.[20] To compare our results to those of Holz et al.,[2] we assumed the tissue area A as a 7-mm diameter circle, since a trephine of the same diameter was used to obtain tissues in their study.

The layer thickness of the ICL, EL, and OCL were measured from three cross-section TEM thin-section images of each eye. The evaluator was unaware of the donor's age when measuring the layer thickness. The measurements were taken with a vernier caliper (BEL-ART Scienceware, Pequannock, NJ) to evaluate the thickness of each layer seen on three ×7500 micrographs of BrM cross sections expanded onto A3+ size (13 ×19 in.) papers. We then measured the layer thickness of five randomly selected locations on each micrograph print. Measurement of the OCL thickness avoided the intercapillary pillars. The thickness of each layer of each eye was determined as the average value of the 15 measurements on the TEM images.

Statistical Analysis

Statistical comparisons between groups were performed by using a two-tailed Student's t-test. Linear regression was used to investigate correlations between variables and to determine correlation coefficients (r) and the significance of such correlations (P). We considered results to be significant at $P < 0.05$.

Results

The results of the stereologic analysis to determine the volume fraction of the images of human BrM prepared by QFDE are listed in Table 2. Variability in the measurements between blocks from the same eye was higher at low-volume fractions than high-volume fractions (data not shown). For $\phi < 0.05$, typical variations were approximately 35%, whereas these variations decreased to approximately 15% for $\phi > 0.05$.

Age-Related Changes of LLP Volume Fraction in Individual Layers

Figure 2 showed the age-related changes of ϕ in the different layers of BrM. The LLP volume fraction of both the ICL ($P = 0.001$) and EL ($P = 0.01$) increased monotonically with donor age (Figs. 2A, 2B). However, unlike the ICL and EL, the ϕ of the OCL appeared to increase before age 60 and then to decrease thereafter (Fig. 2C). Figure 2D shows the data for the OCL, separated into three age groups, with each group covering two decades of donor ages. Use of the Student's t-test indicated significant differences between the averaged ϕ values in both the 20- to 40-year versus the 40- to 60-year ($P = 0.006$) and the

Table 2. D_f and LLP Volume Fraction ϕ Measured by Image Analysis

	ICL		EL		OCL	
Donor Age	D_f (nm)	ϕ	D_f (nm)	ϕ	D_f (nm)	ϕ
27	88.5	0.008	75.1	0.025	98.5	0.009
29	49.5	0.005	79.5	0.009	57.5	0.010
34	78.7	0.005	55.1	0.018	43.4	0.026
35	50.1	0.012	71.0	0.033	58.1	0.011
45	46.5	0.134	73.9	0.131	47.1	0.044
50	71.8	0.031	57.3	0.070	NA	NA
53	59.2	0.051	67.6	0.078	59.9	0.082
58	97.9	0.070	89.2	0.092	88.2	0.086
63	69.5	0.124	58.6	0.126	98.7	0.016
64	59.5	0.099	39.5	0.218	49.3	0.031
77	48.8	0.181	48.7	0.103	57.8	0.054
78	53.9	0.104	43.5	0.099	55.2	0.026

NA, not available.

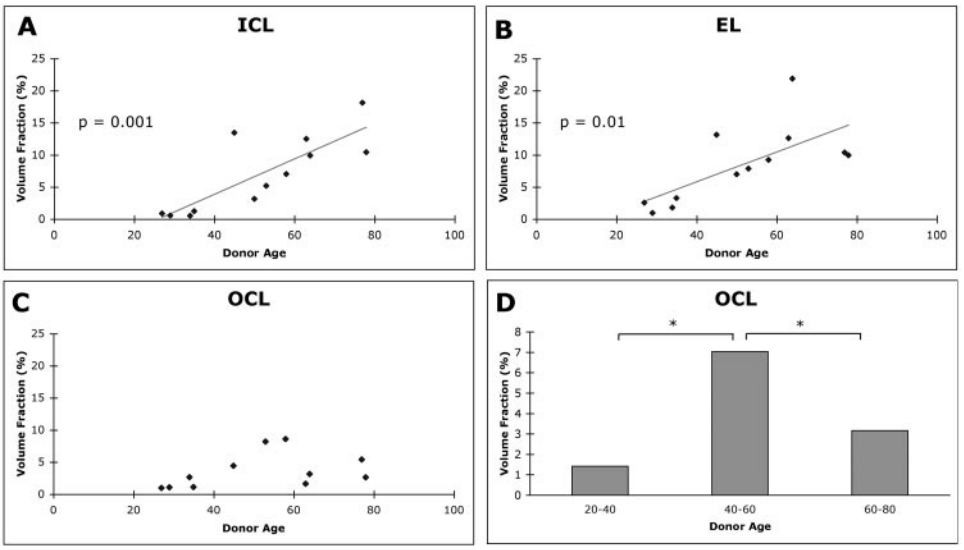

FIGURE 2. The LLP volume fractions as a function of age in the (**A**) ICL, (**B**) EL, and (**C**) OCL of BrM ($n = 12$ for **A** and **B**, $n = 11$ for **C**). (**D**) Comparison of OCL LLP volume fractions among different age groups. *Significant differences.

40- to 60-year versus the 60- to 80-year ($P = 0.046$) groups, showing the highest value of ϕ in the 40- to 60-year group.

Comparison between Layers

In our previous study, we reported that the distribution of LLP depositions appeared different from layer to layer, as did the evolution of these deposits with increasing donor age.[5] To further examine this issue, we compared the ϕ values of the different layers in three groups of eyes, under 40, 40 to 60, and over 60 years. In eyes 20 to 40 years, the ϕ in the EL (2.1% ± 1.0%, mean ± SD, $n = 4$) and OCL (1.4% ± 0.8%, $n = 4$) were higher than in the ICL (0.8% ± 0.3%, $n = 4$; Fig. 3A), with a significant difference seen between the EL and ICL ($P = 0.042$). In the 40- to 60-year group, the ϕ in all three layers was similar, with the EL again having the highest concentration of LLPs (ICL: 7.2% ± 4.5%, $n = 4$; EL: 9.3% ± 2.7%, $n = 4$; OCL: 7.0% ± 2.3%, $n = 3$; Fig. 3B). In the 60- to 80-year group, the ϕ of both the ICL and EL were higher than in the younger eyes (12.7% ± 3.8%, $n = 4$ and 13.7% ± 5.6%, $n = 4$, respectively), and they were significantly higher than the ϕ value of the OCL (3.2% ± 1.6%; $n = 4$; $P = 0.003$ for ICL versus OCL; $P = 0.011$ for EL versus OCL; Fig. 3C).

Total LLP-Associated Lipids in BrM

With the volume fraction ϕ in each of the layers determined, we could evaluate the quantity of LLP-associated lipids in macular BrM of each eye by using equation 3. As the basal lamina of the RPE and choriocapillaris contained very few LLPs,[5] the small contribution of these layers to the total quantity of LLP-associated lipids was not included. Figure 4 shows that the estimated quantity of LLP-associated lipids in BrM (Q) increased with donor age, as expected ($P = 0.001$). Note that these values do not include the LLPs in the lipid walls found in the oldest eyes. We find both the trend and the level of Q (0.6–13.0 μg) are in good agreement with the results for the lipids in BrM/choroid measured by Holz et al.[2]

Size Distribution of LLPs and Age-Related Changes

The age-related changes of average particle diameters D in individual layers are shown in Figure 5. Particle diameters varied in size from approximately 40 to 100 nm without a significant tendency to increase with donor age. Examining the size distribution of the LLPs (Fig. 6) indicated that the distribution of particle size in all three layers broadened between the age ranges 20 to 40 and 40 to 60 years. However, the distribution in the EL and OCL did not appear to change much between age ranges 40 to 60 and 60 to 80 years. We have previously reported that LLPs appear to fuse to form larger particles.[5] Because LLP fusion may be promoted by higher LLP volume fraction, we examined the correlation between the LLP volume fraction and average particle diameter in the different layers. As shown in Figure 7, a significant relationship ($P =$

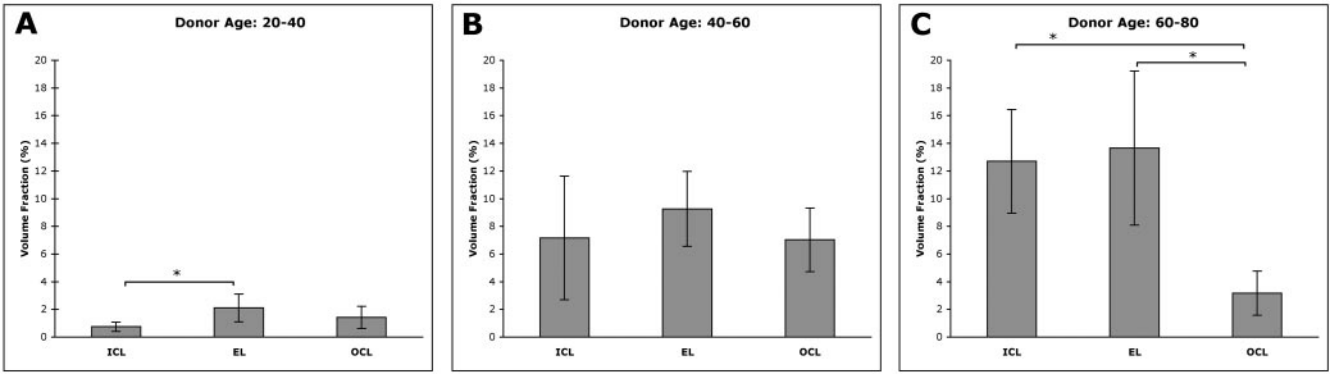

FIGURE 3. Comparison of the LLP volume fractions in the ICL, EL, and OCL of (**A**) 20- to 40-, (**B**) 40- to 60-, and (**C**) 60- to 80-year eyes. Error bars, SD. *Significant differences.

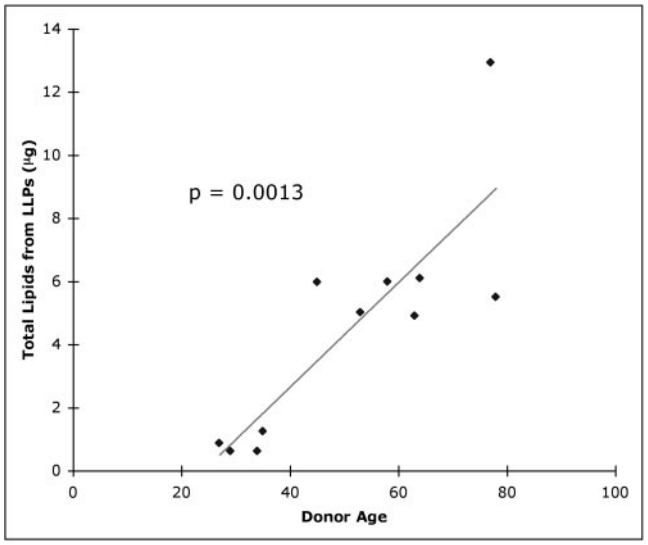

FIGURE 4. The total quantity of LLP-associated lipids in BrM as a function of age.

0.013) was found, but the correlation coefficient between these two parameters is not very strong ($r = 0.41$).

DISCUSSION

In this study, we showed that a major age-related accumulation of LLPs occurred in the ICL and EL of BrM with a lesser accumulation in the OCL (Fig. 2). We did not find a significant increase of the average LLP size with aging. In addition, we were able to estimate the total amount of LLP-associated lipid accumulated in BrM. The estimated lipid amount increased with donor age and was similar to the measurements of the total lipid content of BrM-choroid using a direct assay approach (Fig. 4).[2]

A prominent result of this study was the steady increase of LLP volume fraction with donor age in the ICL and EL (Fig. 2). However, in the OCL, the volume of particles in this region appeared to increase in younger eyes but to decrease in older tissues. The increase of LLP amounts in ICL and EL with age eventually made these two regions the major locations of LLP deposition in BrM (Fig. 3).

The volume fractions of LLP in the different layers were determined based on the assumption that LLPs are spherically shaped objects. Because not all LLPs are spherical, this assumption may introduce some error in the evaluation. If we assume a different shape such as ellipsoidal or cylindrical,[16] we find that the volume fraction of LLPs might be reduced by as much as 10% of the values presented herein (data not shown). However, as most of the LLPs shown in the images appear to be spherically shaped objects, the error in volume fraction due to assumption of particle shape is likely much smaller than 10%.

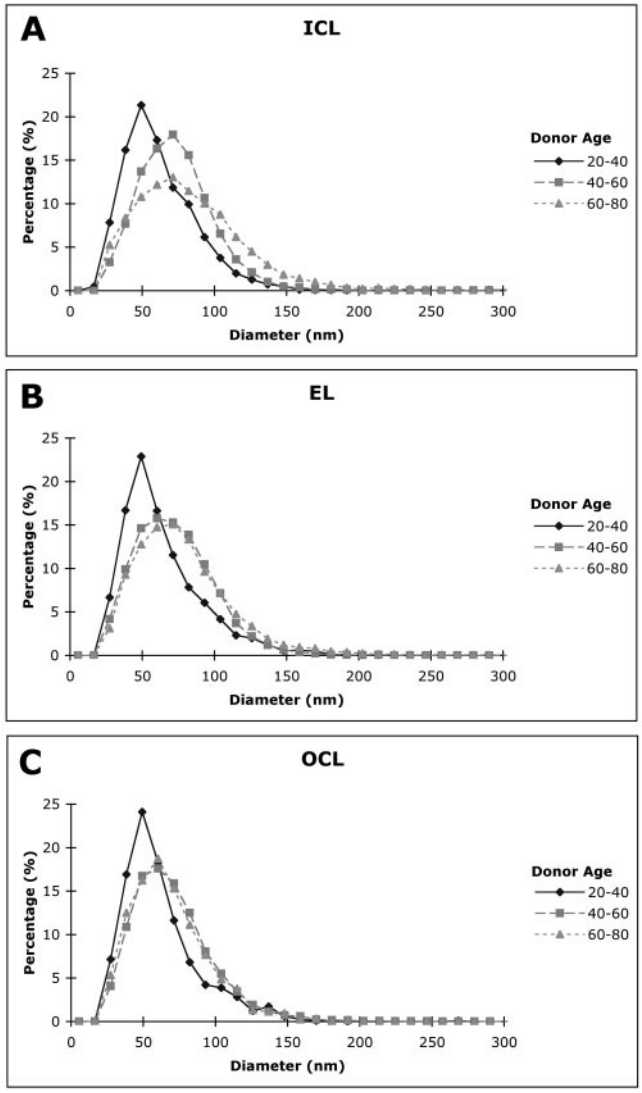

FIGURE 6. The LLP diameter distribution in the different layers of BrM for younger eyes (20–40 years), middle-aged eyes (40–60 years), and older eyes (60–80 years); $n = 4$ for all groups, except $n = 3$ for the OCL in the 40- to 60-year group.

The mechanism causing the inhomogeneous distribution of LLP accumulation in the layers of BrM remains to be deter-

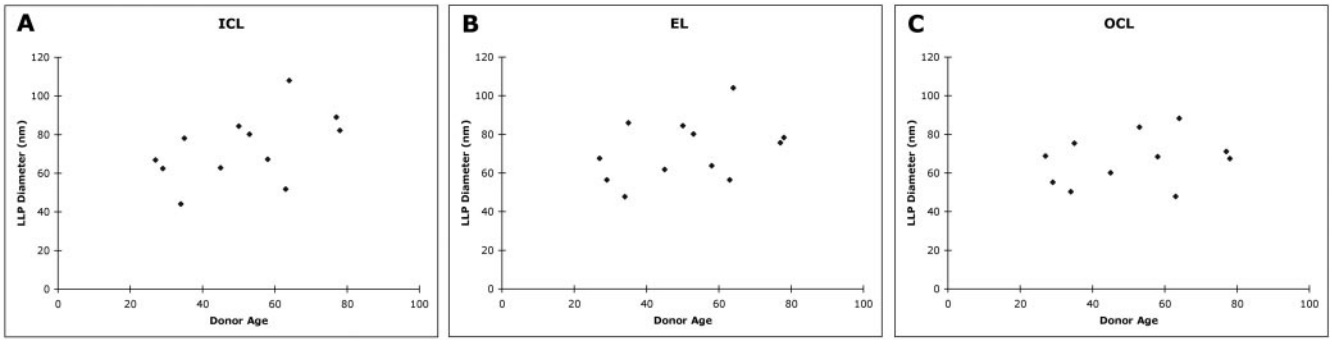

FIGURE 5. The average LLP diameter as a function of age in the (**A**) ICL, (**B**) EL, and (**C**) OCL.

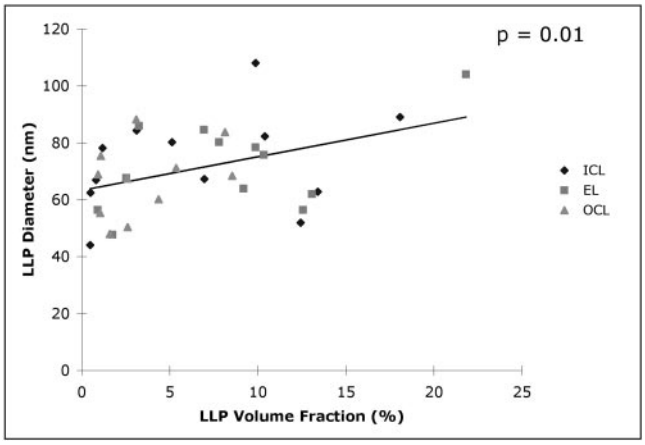

FIGURE 7. LLP particle diameter as a function of volume fraction in the different layers (all eyes).

mined. One explanation may relate to the origin and direction of transport of these particles. In our previous ultrastructural characterization of the LLP accumulation process in BrM, we postulated that the LLPs probably originated as waste products secreted from the RPE for transport to the choriocapillaris. As such, when the interfibrillar spaces of the EL and ICL become filled with LLPs and other debris,[5] further transport through BrM would be limited by this obstruction, and thus LLPs would begin to accumulate in the ICL region, ultimately leading to formation of the lipid wall.

Not only would this mechanism explain the relatively rapid increase in the LLP content of the ICL after age 40, but it may also explain why the age-related change in the volume fraction of LLP in the OCL showed a very different trend (Fig. 2C). Since particles in the OCL still have access to the choriocapillaris and intercapillary pillars, they can be cleared over time from this region, whereas further LLP transport into this region is inhibited by obstruction at the EL.

Support for an RPE origin of LLP particles is found in recent studies of the cholesterol composition of LLPs found in BrM. Li et al.[15] demonstrated that on a density-gradient ultracentrifuge these particles contain a cholesterol profile distinct from that of plasma lipoproteins (including low-density lipoproteins [LDLs]) and postulated that these particles originate in the RPE.

Further support for this theory may come from our findings of the distribution of LLP diameters (Fig. 6). Most of the particles are much larger than the LDL particles (23 nm),[20] even in the youngest eyes examined. This is true in all three layers examined. This result suggests that, unlike other connective tissues in the body,[21] the inclusions seen in BrM are unlikely to be plasma-originated LDLs.

We estimated the total quantity of lipids in the LLP that accumulated with age in BrM by using the volume fraction data and the thickness of each layer measured in donor eyes. Since we selected the highest value of the depth of the field measured in QFDE images and did not include the lipid wall in our calculations, our estimate of lipid amount in macular BrM is conservative. Nevertheless, we found that the quantity of LLP-associated lipids in the tissue increased with age (Fig. 4) and was in a range similar to that of the total lipid amount obtained by a lipid extraction method and in a thin-layer chromatography assay.[2] We caution that this comparison involved assay results that remain to be confirmed, both with regard to the absolute levels[3] and the composition[13,22] of the lipids recovered. Despite these shortcomings, the overall similarity between the morphologic and biochemical results suggests that the LLPs may account for a large portion of the lipids that accumulate with age in BrM.

In our previous work, the density of SGs found in the different layers appeared to increase with age in human eyes.[5] However, due to the small size of these particles and the lack of distinct morphologic features, we were not able to quantify this conclusion in the present study. Hence, the correlation between the accumulation of LLP and SG remains to be determined.

The mechanism of the accumulation of LLPs in BrM remains unknown. Nevertheless, our results suggest that the RPE-originated, lipid-rich materials collect with increasing aging and represent a large portion of lipids found in the tissue. The accumulation of these particles is likely to lead to the formation of a hydrophobic barrier[10] within BrM, compromising the metabolic transport through the area. This particle accumulation is also very likely to be responsible for the age-related increase in hydraulic resistivity that has been reported.[23] Further studies are warranted to investigate the mechanism of deposition and the influence this deposition has on transport processes in this region.

Acknowledgments

The authors thank Zaid Siddik, Melissa F. Chimento, and J. Brett Presley for excellent technical assistance and Robert Linsenmeier (Northwestern University, Evanston, IL) and Howard Kruth (National Institutes of Health, Bethesda, MD) for helpful discussions.

References

1. Pauleikhoff D, Harper CA, Marshall J, Bird AC. Aging changes in Bruch's membrane: a histochemical and morphologic study. *Ophthalmology*. 1990;97:171–178.
2. Holz FG, Sheraidah G, Pauleikhoff D, Bird AC. Analysis of lipid deposits extracted from human macular and peripheral Bruch's membrane. *Arch Ophthalmol*. 1994;112:402–406.
3. Curcio CA, Millican CL, Bailey T, Kruth HS. Accumulation of cholesterol with age in human Bruch's membrane. *Invest Ophthalmol Vis Sci*. 2001;42:265–274.
4. Ruberti JW, Curcio CA, Millican CL, Menco BP, Huang JD, Johnson M. Quick-freeze/deep-etch visualization of age-related lipid accumulation in Bruch's membrane. *Invest Ophthalmol Vis Sci*. 2003; 44:1753–1759.
5. Huang JD, Presley JB, Chimento MF, Curcio CA, Johnson M. Age-related changes in human Bruch's membrane as seen by quick-freeze/deep-etch. *Exp Eye Res*. 2007;85:202–218.
6. Johnson M, Dabholkar A, Huang JD, Presley JB, Chimento MF, Curcio CA. Comparison of morphology of human macular and peripheral Bruch's membrane in old eyes. *Curr Eye Res*. 2007;32: 791–799.
7. Marshall J, Hussain AA, Starita C, Moore DJ, Patmore AL. Ageing and Bruch's membrane. In: Marmor MF, Wolfensberget TJ, eds. *Retinal Pigment Epithelium: Function and Disease.* New York: Oxford University Press; 1998:669–692.
8. Sarks, SH. Ageing and degeneration in the macular region: a clinico-pathological study. *Br J Ophthalmol*. 1976;60:324–341.
9. Grindle CF, Marshall J. Ageing changes in Bruch's membrane and their functional implications. *Trans Ophthalmol Soc UK*. 1978;98: 172–175.
10. Bird AC, Marshall, J. Retinal pigment epithelial detachments in the elderly. *Trans Ophthalmol Soc UK*. 1986;105:674–682.
11. Chen JC, Fitzke FW, Pauleikhoff D, Bird AC. Functional loss in age-related Bruch's membrane change with choroidal perfusion defect. *Invest Ophthalmol Vis Sci*. 1992;33:334–340.
12. Starita C, Hussain AA, Pagliarini S, Marshall J. Hydrodynamics of aging Bruch's membrane: implications for macular disease. *Exp Eye Res*. 1996;62:565–572.
13. Li CM, Chung BH, Presley JB, et al. Lipoprotein-like particles and cholesteryl esters in human Bruch's membrane: initial characterization. *Invest Ophthalmol Vis Sci.* 2005;46:2576–2586.

14. Curcio CA, Presley JB, Millican CL, Medeiros NE. Basal deposits and drusen in eyes with age-related maculopathy: evidence for solid lipid particles. *Exp Eye Res*. 2005;80:761–775.
15. Overby DR, Johnson M. Studies on depth-of-field effects in microscopy supported by numerical simulations. *J Microsc*. 2005;220: 176–189.
16. Overby D, Ruberti J, Gong H, Freddo TF, Johnson M. Specific hydraulic conductivity of corneal stroma as seen by quick-freeze/deep-etch. *J Biomech Eng*. 2001;123:154–161.
17. Tso P, Ragland JB, Sabesin SM. Isolation and characterization of lipoprotein of density less than 1.006 g/ml from rat hepatic lymph. *J Lipid Res*. 1983;24:810–820.
18. Schmitz G, Assmann G, Augustin J, Dirkes-Kersting A, Brennhausen B, Karoff C. Characterization of very low density lipoproteins and intermediate density lipoproteins of normo- and hyperlipidemic apolipoprotein E-2 homozygotes. *J Lipid Res*. 1985;26:316–326.
19. Chapman MJ, Laplaud PM, Luc G, et al. Further resolution of the low density lipoprotein spectrum in normal human plasma: physicochemical characteristics of discrete subspecies separated by density gradient ultracentrifugation. *J Lipid Res*. 1988; 29:442–458.
20. Rifai N, Bachorik PS, Albers JJ. Lipids, lipoproteins, and apolipoproteins. In Burtis CA, Ashwood ER, eds. *Tietz Textbook of Clinical Chemistry*. Philadelphia: W.B. Saunders; 1999:809–861.
21. Smith EB, Slater RS. Relationship between plasma lipids and arterial tissue lipids. *Nutr Metab*. 1973;15:17–26.
22. Haimovici R, Gantz DL, Rumelt S, Freddo TF, Small DM. The lipid composition of drusen, Bruch's membrane, and sclera by hot stage polarizing light microscopy. *Invest Ophthalmol Vis Sci*. 2001;42: 1592–1599.
23. Ethier CR, Johnson M, Ruberti J. Ocular biomechanics and biotransport. *Annu Rev Biomed Eng*. 2004;6:249–273.